8-2010

# Acyl-Chain Mismatch Driven Superlattice Arrangements in DPPC/DLPC/Cholesterol Bilayers

Brian Cannon

Anthony Lewis

Pentti Somerharju

Jorma Virtanen

Juyang Huang

*See next page for additional authors*



## Repository Citation

Cannon, B., Lewis, A., Somerharju, P., Virtanen, J., Huang, J., & Cheng, K.H. (2010). Acyl-chain mismatch driven superlattice arrangements in DPPC/DLPC/cholesterol bilayers. *Journal of Physical Chemistry B, 114*(31), 10105-10113. doi: 10.1021/jp105104f

Published in final edited form as:
*J Phys Chem B*. 2010 August 12; 114(31): 10105–10113. doi:10.1021/jp105104f.

# Acyl-Chain Mismatch Driven Superlattice Arrangements in DPPC/DLPC/Cholesterol Bilayers

**Brian Cannon**[*,†,‡], **Anthony Lewis**[‡], **Pentti Somerharju**[§], **Jorma Virtanen**[⊥], **Juyang Huang**[‡], and **Kwan Hon Cheng**[*,‡]
Department of Chemistry and Biochemistry, The University of Texas at Austin, Austin, Texas 79712, Department of Physics, Texas Tech University, Lubbock, Texas 79409, Institute of Biomedicine, University of Helsinki, Helsinki, Finland, and NanoScience Center, Department of Chemistry, University of Jyväskylä, Jyväskylä, Finland

## Abstract

Fluorescence and infrared spectroscopy and cholesterol oxidase activity were employed to investigate the effect of phosphatidylcholine (PC) acyl chain length mismatch on the lateral organizations of lipids in liquid-ordered dipalmitoyl-PC/dilauroyl-PC/cholesterol (DPPC/DLPC/CHOL) bilayers. Plots of steady-state fluorescence emission anisotropy of diphenylhexatriene (DPH) labeled PC (DPH-PC) embedded in the DPPC/DLPC/CHOL bilayers revealed significant peaks at several DPPC mole fractions ($Y_{DPPC}$) when the cholesterol mole fraction ($X_{CHOL}$) was fixed to particular values. Analogously, the DPH-PC anisotropy peaked at several critical $X_{CHOL}$'s when $Y_{DPPC}$ was fixed. Acyl chain C–H and C=O vibrational peak frequencies of native PC as well as the activity of cholesterol oxidase also revealed dips and peaks at similar $Y_{DPPC}$'s. Importantly, most of the observed peaks/dips coincide with the critical mole fractions predicted by the Superlattice (SL) model. A three-dimensional map of DPH-PC anisotropy versus composition in the range $0.32 \leq X_{CHOL} \leq 0.50$; $0.54 \leq Y_{DPPC} \leq 0.72$ revealed a prominent peak at ($X_{CHOL}$, $Y_{DPPC}$) ≈ (0.42, 0.64). This suggests a simultaneous presence of two different types of superlattices, one where cholesterol is the quest molecule in a PC host lattice and another where DPPC is the guest in the DLPC host lattice. Time-resolved measurements of DPH-PC fluorescence indicated the existence of an ordered, rotationally hindered environment of acyl chains at that "critical" composition consistent with the existence of SL arrangements. We propose that beside CHOL/PC superlattices, DPPC, and DLPC as well tend to adopt regular SL-like lateral distributions relative to each other, presumably because the less hydrophobic DLPC molecule is slightly displaced toward the aqueous phase, thus allowing more room and mobility for the head groups of both DPPC and DLPC as well as for the acyl chain tails of DPPC. The parallel presence of two kinds of superlattices, that is, CHOL/PC-SL and DPPC/DLPC-SL as demonstrated here, has intriguing implications regarding lipid homeostasis of eukaryote membranes.

## Introduction

The cell membrane is a dynamic structure composed of a vast array of different molecules. Cholesterol is a major component of the cell membrane, accounting for as much as 50 mol % of the plasma membrane lipids.[1] In recent years, evidence has accumulated implicating

[*]To whom correspondence should be addressed. (B.C.) Tel: 512-471-1517. Fax: 512-471-2149. brican@mail.utexas.edu. (K.H.C.) Tel: 806-742-3767. Fax: 806-742-1182. kelvin.cheng@ttu.edu.
[†]The University of Texas at Austin
[‡]Texas Tech University
[§]University of Helsinki
[⊥]University of Jyväskylä

that sterol/sphingolipid-rich domains (membrane rafts) may exist in eukaryote membranes.[1,2] Such domains have been proposed to participate in various important cellular functions including lipid and protein sorting and signaling.[3] The principles underlying the formation of such domains as well as the lateral arrangements of lipids therein are not clear, albeit formation of specific cholesterol-phospholipid complexes[4] or regular distributions or superlattices[5,6] has been proposed.

The superlattice (SL) model or regular distribution model[5,6] states that in binary or multicomponent lipid bilayers the lipid molecules tend to adopt regular distributions in the plane of the bilayer to allow for optimal packing both at the headgroup and acyl chain levels. The bilayer free energy is proposed to obtain a local minimum at each SL composition. Intrinsic to the SL model is that (i) only a limited number of allowed critical compositions exist and (ii) between these predictable compositions domains with different SLs coexist together with randomly organized regions. Strong evidence for lipid SLs has been provided by various spectroscopic studies on bilayers of cholesterol and PC[7–9] as well as for phosphatidylethanolamine (PE) and PC bilayers.[10–14]

Rafts or similar lipid domains are likely to contain other lipids (e.g., PC or PE) beside sphingolipid and sterol.[15,16] Therefore, it is necessary to study ternary mixtures to fully understand the principles of formation as well as the architecture of membrane domains. Among such ternary mixtures, the dipalmitoyl-PC/dilauroyl-PC/cholesterol (DPPC/DLPC/CHOL) system has been studied extensively.[17–19] DPPC and DLPC have saturated acyl chains of 16 or 12 carbons, respectively (Figure 1), and the gel-to-liquid crystalline transition temperatures of neat DPPC and DLPC bilayers are 42 and −1 °C, respectively.[18] The phase diagram for DPPC/DLPC/CHOL bilayers have been established.[18–20] It shows the existence of a homogeneous liquid-ordered phase at $0.25 < X_{CHOL} < 0.66$.

Here, we focused on the composition region $0.32 \leq X_{CHOL} \leq 0.50$ and $0.0 \leq Y_{DPPC} \leq 1.0$, where $Y_{DPPC}$ is the DPPC/total PC molar ratio. In this compositional regimen, the bilayer is in the liquid-ordered state and no macroscopic separation of phases have been detected.[18] The system was probed using fluorescence, FTIR, and cholesterol oxidase (COD) activity measurements. Abrupt changes in the spectroscopic parameters of diphenylhexatriene (DPH)-labeled PC (DPH-PC) probe and vibrational frequency of unlabeled PC were observed at several $X_{CHOL}$'s when $Y_{DPPC}$ was fixed and, conversely, at several $Y_{DPPC}$'s when $X_{CHOL}$ was fixed. The majority of those $X_{CHOL}$'s or $Y_{DPPC}$'s coincide with the critical values predicted by the cholesterol/PC or DPPC/DLPC superlattice models, respectively. In addition, simultaneous presence of a cholesterol/PC-SL and a DPPC/DLPC-SL at ($X_{CHOL}$, $Y_{DPPC}$) ≈ (0.42, 0.64) was clearly indicated by a three dimensional (3D) plot of fluorescence anisotropy versus composition as well as time-resolved fluorescence data. Simultaneous presence of two different kinds of superlattices has important implications regarding, for example, the maintenance of lipid compositions of eukaryote membranes.

## Materials and Methods

### Materials

DLPC and DPPC were purchased from Avanti Polar Lipids, Inc. (Alabaster, AL) and cholesterol from Nu Chek Prep, Inc. (Elysian, MN). Lipid purity (>99%) was confirmed by thin layer chromatography (TLC).[7] All organic solvents were of HPLC grade. DPH-PC (1-palmitoyl-2-((2-(4-(6-phenyl-*trans*-1,3,5-hexatrienyl)phenyl)ethyl)carbonyl)-3-*sn*-PC) was obtained from Molecular Probes (Eugene, OR). DPH-PC consists of a 16-carbon saturated fatty acyl chain attached to the *sn*-1 position of the glycerol backbone and a diphenylhexatriene (DPH) fluorophore attached to the *sn*-2 position of the glycerol backbone via a short propanoyl chain (Figure 1). Concentrations of phospholipid stock

solutions were determined by a phosphate assay.[21] Aqueous buffer (pH 7.0, 5 mM PIPES, 200 mM KCl, 1 mM $NaN_3$) was prepared from deionized water (~18 MΩ) and filtered through a 0.1 $\mu$m filter before use. Recombinant cholesterol oxidase (COD) expressed in *E. coli* (C-1235), peroxidase (P-8250) from horseradish and other chemicals for the cholesterol oxidation measurements were purchased from Sigma.

## Preparation of Compositionally Homogenous Liposomes

For both fluorescence and FTIR measurements large multilamellar DPPC/DLPC/CHOL liposomes with or without 0.2 mol % of DPH-PC were prepared using the low-temperature trapping (LTT) technique.[7,9,22] For COD activity measurements, small multilamellar liposomes were prepared using a rapid solvent exchange (RSE) technique.[23,24] The RSE liposomes have a larger surface area-to-volume ratio than those prepared with the LLT method and were therefore preferred for COD activity measurements. After preparation all samples were placed in a 45 °C water bath for 24 h, then slowly cooled to room temperature over a 12 h period. To ensure equilibrium, the liposomes were stored at 23 °C in the dark on a mechanical shaker for at least 10 days before the measurements. The samples were vortexed vigorously once a day during the equilibration period. Previous studies on binary or ternary liposomes prepared by these LTT and RSE methods showed no cholesterol precipitation within the range of $X_{CHOL}$ used here.[14,23,24] TLC analysis did not show detectable degradation of the lipids during equilibration.

## Steady-State and Time-Resolved Fluorescence Measurements

Steady-state fluorescence anisotropy ($r$) based on single photon counting measurements of DPH-PC in DPPC/DLPC/CHOL liposomes were performed on a GREG-PC (ISS Inc., Champaign, IL) fluorometric using a T-mode configuration[25,26] with details given elsewhere.[27] Two separate time-resolved fluorescence (TRF) measurements, total intensity decay $I(t)$, and anisotropy decay $r(t)$, were performed in the frequency-domain[25,28] on an ISS GREG 200 (ISS, Champaign, IL) fluorometer equipped with digital multifrequency cross-correlation phase and modulation acquisition electronics using an L-format. Here, $r(t)$ is defined as $(I_{//}(t) - I_{\perp}(t))/(I_{//}(t) + 2I_{\perp}(t))$, where $I_{//}(t)$ and $I_{\perp}(t)$ are the fluorescence decays of the parallel and perpendicular polarized emissions, respectively, of DPH-PC upon excitation by a parallel polarized delta-pulse of light.[25,29] Detailed descriptions of nanosecond-resolved fluorescence intensity and anisotropy decay measurements in the frequency-domain have been described in detail elsewhere.[25,26,28] The sample was also under constant stirring with a magnetic bar during the time-resolved measurements. It is important to mention that the noise level in the raw frequency domain data and emission spectra of DPH-PC after more than 10 days of equilibration at 23 °C were similar to those immediately, or a few days after the sample preparation (results not shown). These observations suggest that no significant degradation of the fluorescent probe took place during the ≥10 day equilibration period.

## Analysis of Time-Resolved Fluorescence Data

The mean fluorescence lifetime ($\tau$) was calculated from the frequency-domain intensity data using a simple biexponential decay model.[9,25] Using a first-order rotational dynamics model that assumes isotropic rotation of DPH in lipid bilayers, a single rotational correlation time ($\rho$) of DPH-PC was recovered from the lifetime and steady-state anisotropy measurements using the Perrin equation[30] according to eq 1

$$r = \frac{r_o}{1 + (\tau/\rho)} \quad (1)$$

Here $r_0$ is the initial anisotropy, which is 0.34 for DPH-PC in a lipid environment at room temperature.[26] For a higher-order rotational dynamics analysis of DPH-PC, a wobbling diffusion model[31] was used to fit the frequency-domain anisotropy decay $r(t)$ data. The order parameter ($S$) and rotational diffusion rate ($D$) of DPH-PC in lipid bilayers were obtained using eq 2

$$r(t)=r_o[(1-S^2)e^{-6Dt/(1-S^2)}+S^2] \quad (2)$$

The order parameter $S$, which can vary from 0 to 1, describes the orientational order of the probe relative to the normal of the lipid membranes. The localized rotational diffusion constant ($D$) describes the rate of wobbling diffusion of the probe among the acyl chains of the matrix lipid. It is important to mention that the steady state anisotropy $r$ is related with $I(t)$ and $r(t)$ according to eq 3[31]

$$r=\frac{\int_0^\infty r(t)I(t)\mathrm{d}t}{\int_0^\infty I(t)\mathrm{d}t} \quad (3)$$

Therefore, $r$ provides information on both on the fluorescence decay and rotational dynamics of the probe.

## FTIR Measurements

The liposomes were prepared as for fluorescence measurements except that the total concentration of lipids was 400 $\mu$M and no DPH-PC was included. After ≥10 days of equilibration at 23 °C, the liposomes were pelleted by centrifugation at 20 000 × $g$ for 20 min at 23 °C and then applied on a single reflection horizontal attenuated total reflectance (ATR) sample cell (Pike Technologies, Inc., Madison, WI) kept at 23 °C. Infrared spectra were recorded with a Magna-IR 560 FTIR spectrometer (Nicolet Inc., Madison, WI) equipped with a deuteriated triglycine sulfate detector operated at room temperature. Typically, 50 interferograms with 1 $cm^{-1}$ resolution were collected, averaged, Fourier transformed and background subtracted[9] with the Omnic Software provided by Nicolet. Contributions by water and cholesterol were subtracted using published procedures.[9,32]

## Measurement of Cholesterol Oxidase Activity

The initial rate of oxidation of cholesterol in DPPC/DLPC/CHOL bilayers by COD was determined photometrically using a coupled-enzyme assay as detailed previously.[14]

## Data Smoothing and Statistical Significance of Deviations

Several parallel sample sets, each independently prepared by the LTT or RSE method, were used in the fluorescence (steady state and TRF), FTIR, and COD-mediated cholesterol oxidation studies. Spectroscopic measurements (i.e., $r$ of DPH-PC, IR vibrational bands of PC and COD activities) from different parallel sample sets as a function of lipid composition were collected spearately. The primary data sets consisted of data points representing averages of data from parallel sample sets. Additional smoothed data sets, one-pass and two-pass 3-point running averages were subsequently generated. Smoothing was used to help in detecting dips, peaks, or other deviations in the primary data plots. Since the relative accuracy of the $X_{CHOL}$ and $Y_{DPPC}$ values is about ±0.03, only the deviations defined by two or more primary data points were generally considered relevant.[9] The locations of the dips

or peaks in the spectroscopic parameter versus composition plots were determined from the minima or maxima of the two-pass 3-point running averages, respectively.

Statistical significance of the peaks and dips in the measured parameters versus compositions was analyzed using a unidirectional *t*-test of unequal variances.[27,33,30,33] In this study, the two means represented the mean of the peak or dip ($y_c$) at the "critical" and the mean of the adjacent or baseline value ($y_b$) of a nearby primary point obtained from independently prepared parallel samples. The probability ($P$) of rejecting the null hypothesis of the two means being identical, that is, $y_c = y_b$, was calculated from the *t*-test and detailed elsewhere.[9,33] Here, the statistical significance of the peak or dip value as compared with two baseline values is therefore given by $P_L$ and $P_R$, representing the probabilities that the spectroscopic parameter value corresponding to a dip or peak is different from the adjacent starting (left) and ending (right) sides of the dip (or peak), respectively. Raw rather than averaged or smoothed data sets were used in the statistical analysis. Peaks or dips with $P_L$ or $P_R$ less than 70% were ignored in this study. Although this 70% cutoff is arbitrary, it together with $P_L$ and $P_R$ provide a standard gauge to examine and cross-compare the "critical" changes of the direct and recovered parameters obtained from the measurements.

### Superlattice Theory of DPPC/DLPC/CHOL Bilayers

The superlattice (SL) model proposes that two phospholipids with different molecular structures tend to adopt hexagonal (HX), centered rectangular (CR) or rectangular (R), superlattice-like distributions in mixed bilayers.[10–12] DPPC and DLPC differ in respect to acyl chain length (Figure 1), which could drive SL arrangements based on factors indicated in Discussion. SL formation can be deduced from abrupt changes in bilayer properties at certain, predictable (critical) values of the DPPC/(DPPC + DLPC) ratio ($Y_{DPPC}$), which can be derived based on simple geometrical principles.[10] The critical $Y_{DPPC}$'s for superlattices with a hexagonal (HX), centered rectangular (CR) or rectangular (R) symmetry, that is, $Y^{HX}$, $Y^{CR}$, or $Y^{R}$, respectively, are given by the equations $1/((a^2 + ab + b^2)$, $1/(2ab + b^2)$, or $1/(ab + b^2/2)$, respectively, when $Y_{DPPC} < 0.5$.[34] When $Y_{DPPC} > 0.5$, the roles DPPC and DLPC are reversed, that is, DLPC is host and DPPC is the guest molecule. Then the corresponding critical $Y_{DPPC}$'s are given by eqs $1 - 1/((a^2 + ab + b^2)$, $1 - 1/(2ab + b^2)$, or $1 - 1/(ab + b^2/2)$, respectively,.[34] In these equations $a$ and $b$ are lattice coordinates, that is, the distance in lattice sites between two proximal guest molecules along the principal lattice axes.[34] Each DPPC/DLPC-SL is therefore uniquely identified by the lattice coordinates ($a$, $b$). The critical compositions of such SL's are identical to that of the Headgroup-SL.[10,12,34]

On the other hand, at the acyl chain level where the SL consists of cholesterol and phospholipid, cholesterol is the guest and the acyl chains are the hosts. The critical mole fraction of cholesterol $X_{CHOL}$ defined as cholesterol-to-lipid ratio, for superlattices corresponding to a HX and CR and R symmetries is given by $2/(a^2 + ab + b^2 + 1)$, $2/(1 + 2ab + b^2)$, or $2/(1 + ab + b^2/2)$, respectively. Some predicted critical $X_{CHOL}$ values in cholesterol/PC-superlattices (CHOL/PC-SL) (when $X_{CHOL} \geq 0.20$) are 0.200, 0.220, 0.250, 0.286, 0.333, 0.400, 0.500, and 0.667.[9,35]

## Results

Figure 1 shows the molecular structures of the lipids used in this study, that is, DPPC, DLPC, DPH-PC, and cholesterol. The fluorescent DPH-PC is similar to DPPC as far as the molecule length is concerned, while the length of DLPC is four-carbons less that that of DPPC. Thus, there is significant mismatch of hydrophobic lengths between DPPC and DLPC in mixed bilayers. The hydrophobic length of cholesterol is similar to that of DPPC.

### Steady-State Fluorescence Anisotropy Measurements

Figure 2A–C shows the steady-state fluorescence anisotropy ($r$) of DPH-PC in DPPC/DLPC/CHOL liposomes as a function of $X_{CHOL}$ with an increment of 0.01 with $Y_{DPPC}$ fixed to 0.50, 0.60, or 0.66. Primary data, which are averages of three parallel sets, one-pass as well as two-pass running averages are shown. For each fixed $Y_{DPPC}$, peaks are evident in the two-pass running average plots. As described in Materials and Methods, peaks were considered relevant only if defined by at least two primary data points with $P_L$ and $P_R$ values of at least 70%. Table 1 summarizes the $X_{CHOL}$ values of the peaks and the corresponding ($P_L$, $P_R$) values for each fixed $Y_{DPPC}$. In addition, relevant predicted critical cholesterol mole fractions ($X^{HX}$, $X^{CR}$, and $X^R$) are listed. Notably, peaks at $X_{CHOL} \approx 0.31$, 0.42, and 0.55 were consistently found for each fixed $Y_{DPPC}$. In addition, peaks were detected at $X_{CHOL} \approx 0.15$, 0.20, 0.26, and 0.52 for some, but not each fixed $Y_{DPPC}$. Except $X_{CHOL} \approx 0.55$, the peaks found coincide with $X^{HX}$, $X^{CR}$, or $X^R$ within ±0.03 mol fraction (Table 1). In summary, 11 out of 14 of the significant $r$ peak locations coincide with critical mole fractions predicted by the CHOL/PC-SL model.

Figure 2D–F shows plots of $r$ versus $Y_{DPPC}$ with an increment of 0.02 for a fixed $X_{CHOL}$ of 0.35, 0.40, or 0.45. For each fixed $X_{CHOL}$, peaks were evident in the two-pass running average plots. Table 2 summarizes $Y_{DPPC}$'s of the peaks and the corresponding ($P_L$, $P_R$) values. The relevant predicted critical mole fractions, that is, $Y^{HX}$, $Y^{CR}$, and $Y^R$ are also listed. Two significant peaks at $Y_{DPPC} \approx 0.66$ and 0.83 were consistently found for each three fixed $X_{CHOL}$, while peaks at $Y_{DPPC} \approx 0.15$, 0.20, 0.30, 0.46, 0.51, and 0.56 were found for some, but not all fixed $X_{CHOL}$'s. Except for those at $Y_{DPPC} \approx 0.46$ and 0.56, all peaks agree with theoretical $Y^{HX}$, $Y^{CR}$, and $Y^R$ values within ±0.03 (Table 2). Altogether, 12 out of 14 of the $r$ peaks coincide with critical mole fractions predicted by the DPPC/DLPC-SL model. All the significant peaks indicated above were consistently observed after 9 days of sample preparation and the data were systematically collected exactly after 10 days of incubation.

The "critical" $X_{CHOL} \approx 0.56$ (Figure 2) is not predicted by the CHOL/PC-SL model. However, DPH-PC anisotropy measurements with dioleoyl-PC/cholesterol (DOPC/CHOL) bilayers have shown a deviation close to $X_{CHOL} = 0.57$ in a previous study,[7] and the chemical potential of cholesterol, as measured with a cholesterol oxidase (COD) assay,[24] also showed an abrupt increase at $X_{CHOL} = 0.57$ in several binary DOPC/CHOL, DPPC/CHOL, and 1-palmitoyl, 2-oleoyl-PC/CHOL bilayers. In addition, Monte Carlo simulations based on an Umbrella model indicated that a cholesterol-dimer superlattices structure exists at $X_{CHOL} = 0.57$.[7,22] In addition, the above Monte Carlo simulations also support regular distribution (SL) of cholesterol at $X_{CHOL} = 0.154$, 0.25, 0.40, 0.5 as shown in Table 1.

Tables 1 and 2 demonstrated that peaks or "critical" compositions at $X_{CHOL} \approx 0.38$–0.43 and at $Y_{DPPC} \approx 0.64$–0.68 with the average ($P_L$, $P_R$) values of (86, 92) and (93, 92), respectively, were consistently detected by steady-state DPH-PC fluorescence anisotropy measurements. This suggested to us that a complex DPH-PC anisotropy landscape may exist close to those compositions. Therefore, these "critical" compositional coordinates were in the focus of a consequent, more detailed mapping of the DPH-PC anisotropy versus vs composition. One hundred independent data points, each an average of three parallel independently prepared samples, covering the region $0.32 \leq X_{CHOL} \leq 0.50$ and $0.54 \leq Y_{DPPC} \leq 0.72$ were obtained (Figure 3). A clear anisotropy peak at ($X_{CHOL}$, $Y_{DPPC}$) ≈ (0.42, 0.64) in this 3D anisotropy map is obvious.

### Time-Resolved Fluorescence Measurements

To explore the rotational dynamics of DPH-PC around the anisotropy peak at ($X_{CHOL}$, $Y_{DPPC}$) ≈ (0.42, 0.64), we carried out time-resolved fluorescence (TRF) measurements on DPH-PC incorporated in DPPC/DLPC/CHOL bilayers. Twelve different lipid compositions were examined and values of intensity decay ($\tau$), rotational correlation time ($\rho$), orientational order ($S$) and rotational diffusion coefficient ($D$) were extracted as outlined in Materials and Methods. When $Y_{DPPC}$ was fixed to 0.64, no significant changes in $\tau$ were observed as a function of $X_{CHOL}$ (Figure 4A). Neither were significant deviations observed in $\tau$ with increasing $Y_{DPPC}$ when $X_{CHOL}$ was fixed to 0.42 (Figure 4C). When the Perrin equation (eq 1) was employed, $\rho$ exhibited a peak at $X_{CHOL}$ ≈ 0.42–0.44 when $Y_{DPPC}$ was fixed to 0.64 (Figure 4A), and at $Y_{DPPC}$ ≈ 0.62 for $X_{CHOL}$ fixed to 0.42 (Figure 4C). Using a more detailed rotational model (eq 2), a peak in $S$ and a dip in $D$ were observed at $X_{CHOL}$ ≈ 0.40 for $Y_{DPPC}$ fixed to 0.64 (Figure 4B), and at $Y_{DPPC}$ ≈ 0.62–0.64 for $X_{CHOL}$ fixed to 0.42 (Figure 4D). The peak or dip locations from the TRF parameter versus $X_{CHOL}$ or $Y_{DPPC}$ therefore coincide with anisotropy peak at ($X_{CHOL}$, $Y_{DPPC}$) ≈ (0.42, 0.64) in the 3D-plot of Figure 3. In addition, the TRF data indicate a more highly ordered, rotationally hindered environment of the DPH moiety at ($X_{CHOL}$, $Y_{DPPC}$) ≈ (0.42, 0.64) as compared to other compositions.

### FTIR Measurements

FTIR measurements of DPPC/DLPC/CHOL liposomes devoid of DPH-PC were performed next using five parallel, independently prepared data sets. While cholesterol does not absorb in the region of the C=O vibrational bands, its C–H bands overlap with the symmetric C–H bands of lipid acyl chains at ~2850 $cm^{-1}$. However, the cholesterol-specific band at ~1365 $cm^{-1}$ allows one to subtract cholesterol contribution from the intensities of the C–H bands of DLPC and DPPC.[9,32] Figure 5 shows the frequencies of the symmetric C–H (Figure 4A) and C=O (Figure 4B) bands versus DPPC content when $X_{CHOL}$ was fixed to 0.40. The frequency of the C–H band decreased with increasing $Y_{DPPC}$, and significant dips, or "critical" $Y_{DPPC}$ mole fractions, were detectable at $Y_{DPPC}$ ≈ 0.12, 0.48, and 0.68. The minimum at $Y_{DPPC}$ = 0.84 is not considered as a significant dip, since at least two data points were required to define a significant deviation (see Materials and Methods). In case of the C=O band, the vibrational frequency peak decreased slightly with increasing DPPC content for $Y_{DPPC}$ = 0 to 0.88 and significant deviations were observed at $Y_{DPPC}$ ≈ 0.10, 0.36, 0.48, and 0.68. At $Y_{DPPC}$ of 0.88–1.00, a sharp decrease in the C=O frequency with increasing DPPC fraction is evident. Table 3 summarizes the $Y_{DPPC}$ values at which significant deviations were observed in the FTIR measurements, along with the critical mole fractions $Y^{HX}$, $Y^{CR}$, and $Y^{R}$ predicted by the DPPC/DLPC-SL model. Notably, all observed deviations agree closely (±0.03) with predicted $Y^{HX}$, $Y^{CR}$, and $Y^{R}$ vales, and a deviations at $Y_{DPPC}$ ≈ 0.68 was observed in the C–H as well as C=O plots.

### Activity of Cholesterol Oxidase versus $Y_{DPPC}$ at $X_{CHOL}$ of 0.40

The initial rate of oxidation of cholesterol by COD in DPPC/DLPC/CHOL liposomes was determined as described in Materials and Methods. Figure 6 shows the rate of cholesterol oxidation as a function of $Y_{DPPC}$ at a fixed $X_{CHOL}$ of 0.40. Because of the low activity of COD in this system the noise level was relatively high and thus altogether 11 parallel independently prepared sample sets were examined. Table 3 summarizes the locations of the peaks and the respective values of ($P_L$, $P_R$). Only the two major peaks at $Y_{DPPC}$ ≈ 0.64 and 0.80 coincide with the predicted $Y_{DPPC}$ values from the DPPC/DLPC-SL model.

## Discussion

### Phase Behavior of DPPC/DLPC/CHOL Bilayers

Previous studies[18–20] of the phase diagram of DPPC/DLPC/CHOL revealed the existence of several phases and boundaries. Briefly, there are four regions depending on cholesterol mole fraction. Region I ($X_{CHOL} < 0.16$) consists of three phases, (i) a DLPC-rich fluid lamellar phase at low $Y_{DPPC}$, (ii) a DPPC-rich ordered lamellar phase at high $Y_{DPPC}$, and (iii) a coexisting mixed fluid and ordered lamellar phase at intermediate $Y_{DPPC}$. Region II ($0.16 < X_{CHOL} < 0.25$) is a one-phase ordered and fluid nanodomains region, where the properties of the lipid mixtures change continuously as a function of $Y_{DPPC}$. Region III ($0.25 < X_{CHOL} < 0.66$) consists of a homogeneous liquid-ordered phase. Lastly, region IV ($X_{CHOL} > 0.66$) consists of a cholesterol-saturated liquid-ordered phase coexisting with cholesterol monohydrate crystals not associated with the bilayer. Thus "critical" $X_{CHOL}$'s, that is, those at which peaks or dips in measured parameters were observed (Table 1), as well as the "critical" $Y_{DPPC}$'s at a fixed $X_{CHOL} = 0.35$, 0.40, and 0.45 (Table 2), lie within the cholesterol regimen where only a homogeneous one-phase region (II or III) exist. The "critical" $X_{CHOL} \approx 0.15$ at a fixed $Y_{DPPC}$ of 0.50 is an exception and could be considered to lie at the phase boundary between Region I and Region II. All "critical" $Y_{DPPC}$'s are lie in the homogeneous Region III.

### Evidence for Coexisting Cholesterol/PC and DPPC/DLPC Superlattices

The superlattice (SL) model states that lipids in binary or multicomponent membranes tend to adopt regular, superlattice-like distributions, which are energetically more favorable than the other, intervening compositions. Indicative of SL formation is the presence of abrupt changes (peaks, dips, or kinks) in plots of a physical parameter or enzyme activity at predictable critical compositions.[5,6]

Here, we used fluorescence spectroscopy, FTIR, and cholesterol oxidase activity measurements to investigate superlattice formation in DPPC/DLPC/CHOL bilayers. Tables 1 and 2 compare the statistically significant peaks in steady state anisotropy of DPH-PC versus composition plots with critical compositions predicted by SL model (Figure 2). Approximately 80% of the observed "critical" $X_{CHOL}$'s or $Y_{DPPC}$'s revealed by fluorescence measurements agree with the critical mole fractions predicted by assuming the formation of CHOL/PC or DPPC/DLPC superlattices, respectively. Note that a recent work on DPH fluorescence anisotropy measurements[36] in binary cholesterol/1-palmitoyl, 2-oleoyl-PC (CHOL/POPC) liposomes reveal distinct peaks at $X_{CHOL} = 0.200$, 0.220, 0.250, and 0.262 and agree favorably (±0.03) with our DPH-PC measurements as shown in Figure 2. Table 3 shows an analogous comparison of predicted values with those revealed by FTIR or COD activity measurements. While only 50% of the "critical" $Y_{DPPC}$'s revealed by the COD activity measurements agree with those predicted by the SL model, all of the "critical" $Y_{DPPC}$'s revealed by FTIR measurements agree with predicted ones. Notably the "critical" $X_{CHOL} \approx 0.38$–0.42 and $Y_{DPPC} \approx 0.64$–0.68 were detected by all three different techniques, consistent with a strong tendency for superlattice formation at those compositions.

Our present and previous investigations on binary[7,9,11,12] or ternary[14,27,37] systems detected all the critical compositions predicted by the SL model. This may be due to (i) perturbation of lateral organization locally by the fluorescent probes used, (ii) lack of sensitivity of the detection methods for subtle changes in bilayer properties, or (iii) low stability of some superlattice arrangements. On the other hand, "critical" compositions that do not do not agree with the superlattice model have been observed.[5,6] This might be due to experimental artifacts, such as perturbation of bilayer structure by the probe used (e.g., bulky DPH fluorophore) or by the COD enzyme.[14] Note that a recent work[36] on the excitation

generalized polarization of 6-lauroyl-2-(dimethylamino)naphthalene fluorescence in binary CHOL/POPC liposomes revealed biphasic changes at all the critical compositions predicted by the SL model in the range of $X_{CHOL}$ = 0.18 to 0.52.

DPH-PC is a useful probe when investigating lateral heterogeneity and molecular dynamics of lipid bilayers.[38] The 3D steady-state anisotropy plot (Figure 3) revealed a prominent peak at ($X_{CHOL}$, $Y_{DPPC}$) of ~(0.42, 0.64) thus implicating simultaneous presence of CHOL/PC and DPPC/DLPC superlattices. The fact that the fluorescence lifetime was independent of the composition across the peak and in its vicinity (Figure 4A,C) suggests that this peak relates to superlattice formation rather than phase separation. Phase separation is also not consistent with the published phase diagram (see above). Previous work on DPH-PC in binary PC/CHOL bilayers demonstrated a strong decrease in the fluorescence lifetime when DPH-PC was present in poorly packed regions existing at domain boundaries.[9] An increase in the rotation correlation time (Figure 4A,C) and the concomitant increase in the orientational order and decrease in the diffusion coefficient of DPH-PC (Figure 4B,D) occurs at ($X_{CHOL}$, $Y_{DPPC}$) = (0.42, 0.64), presumably due to simultaneous presence of CHOL/PC and DPPC/DLPC superlattices at this composition.

FTIR spectroscopy provides a probe-independent method to monitor mobility/conformation of specific lipid residues in bilayers. FTIR measurements on DPPC/DLPC/CHOL bilayers with $X_{CHOL}$ = 0.40 revealed deviations at $Y_{DPPC} \approx$ 0.12, 0.48, 0.68. The overall decrease of the C–H band frequency with increasing DPPC content indicates that an increase in the acyl chain order occurs when the mole fraction of DLPC having short 12:0 chains decreases at the expense of increasing DPPC with the longer 16:0 chains. The observed increase in acyl chain order with increasing $Y_{DPPC}$ could result from the enhanced condensing effect by cholesterol due to its long axis orienting closer to the membrane normal. The presence of dips in C–H frequency at predicted critical compositions is consistent with SL formation, since the tighter packing of lipids in superlattices[9,39] is expected to reduce the proportion of gauche rotamers.

The C=O band frequency is thought to be sensitive to hydration and/or conformation of the interfacial carbonyl regions.[9] Besides the “critical” $Y_{DPPC} \approx$ 0.12, 0.48, 0.64 revealed by the C–H frequency, another critical $Y_{DPPC} \approx$ 0.36 is evident in the $C$ = O frequency plot and falls close to critical $Y_{DPPC}$ of 0.33 predicted by the DPPC/DLPC-SL model. An increase in either conformational disorder or hydration of the carbonyl groups could be responsible for this dip in the $C$ = O frequency versus composition plot. An increase in conformational order at a predicted critical composition would be consistent with superlattice formation. Notably, the presence of a critical composition at $Y_{DPPC} \approx$ 0.68 in all FTIR plots is consistent with the florescence data discussed above.

## Factors Driving the Formation of DPPC/DLPC Superlattices

Formation of superlattice arrangements in 1-palmitoyl, 2-oleoyl-PE/1-palmitoyl, 2-oleoyl-PC (POPE/POPC) bilayers in the absence[11,12] and presence[13,14] of cholesterol studied previously can be understood based on the fact that the effective size of the headgroup of POPE is much smaller than that of POPC, that is, POPE acts as a spacer relieving steric strain caused by close packing of the larger head groups of POPC. Obviously, the spacer effect is most efficient when POPE adopts a regular, SL-like lateral distribution. Since the head groups of DPPC and DLPC are identical, it may seem unlikely that interactions at the headgroup level could drive SL formation in this system. However, it is possible that the transverse (along the normal of the bilayer plane) distributions of the head groups of DPPC and DPLC may not be identical, that is, the headgroup of DPLC could be slightly displaced toward the aqueous phase as compared to the headgroup of DPPC. Such a transverse displacement would be due to the much lower hydrophobicity of DLPC as compared to

DPPC, which is shown by a previous study[40] that the spontaneous interbilayer transfer of DLPC is approximately 4000 times faster than that of DPPC based on measured rates of analogous lipids. In addition, recent studies with A-type phospholipases showed that the hydrolysis of DLPC is much faster than that of DPPC in fluid, multicomponent bilayers.[41] This result can be explained by that the phospholipid substrate has to efflux from the bilayer to reach the active site of the enzyme, which is located well above the bilayer surface. Hence, efflux of DLPC molecules would be more facile than that of DPPC molecules if they were located higher in the bilayer to start with. The degree of headgroup displacement is not known, but it appears that only a minor displacement would result in a significant relief of steric strain at the headgroup level, thus providing a driving force for formation of DPPC/DLPC superlattices. An additional factor could be that the shorter lauroyl chains of DLPC would create a void near the bilayer center. This would provide more space for the tails of the longer palmitoyl chains of DPPC, which, like diminished strain at the headgroup level, would be entropically favorable. It is notable that the presence of cholesterol is a prerequisite for the formation of DPPC/DLPC superlattices, since without cholesterol DPPC and DPLC would be phase separated (see above).

Preferential interactions of cholesterol with PC of different chain lengths may also be a factor in regulating the lateral organization of bilayers. Previous thermodynamic measurements[20] have indicated that cholesterol may preferentially interact with DPPC over DLPC due to a lesser degree of hydrophobic mismatch with cholesterol. In a similar system with hydrophobic mismatch between two PCs and in the presence 40% cholesterol, a nearest-neighbor recognition method suggested that cholesterol prefers to associate with PC of longer chains.[42] A previous MD simulations study[43] on a binary PC/CHOL further suggested the existence of a “charge pair” as a possible mode of interaction between the cholesterol hydroxyl group and the ammonium group of the PC headgroup as such an inward orientation of the PC headgroup is preferred. Also, such interaction has been shown to be more likely at 40% cholesterol content in DPPC bilayers than in DLPC bilayers as a result of a larger cholesterol tilt toward the carbonyl region due to hydrophobic mismatch of cholesterol and DLPC acyl chains.[44]

## Comparison of POPE/POPC/CHOL and DPPC/DLPC/CHOL Superlattices

In our previous study on the ternary POPE/POPC/CHOL system, an increase in the rotational diffusion and a decrease in order (as reported by DPH-PC) as well as a decrease in the acyl chain conformational order (as detected by FTIR) were observed at $X_{CHOL} \approx 0.40$; $Y_{POPE} \approx 0.68$.[27] In the present study, these parameters changed in opposite direction at the “critical” compositions of $X_{CHOL} \approx 0.42$ and $Y_{DPPC} \approx 0.64$. While the lateral organization of cholesterol and phospholipid molecules are predicted to be equivalent in both systems (cf. Figure 7 and Figure 10 in Cannon et al. 2006[27]), significant differences in the interactions among lipids exist. In POPE/POPC/CHOL bilayers the CHOL/PC-SL and POPE/POPC-SL are coupled at the headgroup level since both POPE and POPC have identical acyl chain compositions but different headgroup structures. In DPPC/DLPC/CHOL bilayers CHOL/PC-SL and DPPC/DLPC-SL are coupled at the acyl chain level since DPPC and DLPC have identical headgroup structure but different acyl chain lengths (or hydrophobic mismatch). Hence, the “critical” mole fractions in the POPE/POPC/CHOL bilayers are associated with the headgroup interactions while those in the DPPC/DLPC/CHOL with the acyl-chain mismatch. Both types of SLs share identical lateral organizations, and the presence of simultaneous CHOL/PC-SL and POPE/POPC-SL was also observed at similar critical mole fractions, that is, $X_{CHOL} \approx 0.40$ and $Y_{DPPC} \approx 0.68$ using an identical DPH-PC lipid probe. In addition, using similar fluorescence, FTIR and COD measurements in both POPE/POPC/CHOL[14,27] and DPPC/DLPC/CHOL systems, common “critical” phospholipid compositions were detectable at ~0.19–0.22, 0.32–0.36, 0.47–0.53, 0.64–0.68 at a fixed

$X_{CHOL}$ = 0.40, although the definition of compositions are different, that is, POPE/(POPC + POPE) and DPPC/(DPPC + DLPC), respectively.

### Biological Relevance of Superlattice Formation

The most intriguing aspect of lipid superlattices is that they may be key players in the regulation of the lipid composition of biological membranes. First, since the critical (superlattice) compositions represent local energy minima along the compositional axis, the lipid composition of a membrane has an intrinsic tendency to settle in such a composition. The critical compositions would thus act as set-points. Second, a deviation of the composition from a critical one will lead to the formation of poorly packed regions at domain boundaries, and phospholipids residing in such regions are known to be particularly susceptible for phospholipase-mediated hydrolysis.[45] Hydrolysis of the phospholipid species in excess by a homeostatic phospholipase would restore the critical composition and, consequently, the poorly packed domains would disappear thus preventing further hydrolysis by the phospholipase. Third, also biosynthetic enzymes could be activated/inactivated by the abrupt changes occurring in bilayer organization at or close to critical compositions.[6] Superlattices could also regulate the cholesterol content of membranes. It has been proposed that if the cholesterol/phospholipid ratio exceeds a “critical” value, the chemical activity (or fugacity) of cholesterol increases abruptly, which in turn increase cholesterol efflux from that membrane or increases its esterification by acyl-cholesterol acyltransferase.[46]

## Conclusions

Using complementary fluorescence, FTIR, and cholesterol oxidase activity measurements, this study demonstrates that superlattices due to CHOL/PC at the tail group region and DPPC/DLPC due to hydrophobic mismatch in ternary DPPC/DLPC/CHOL bilayers exist. The presence of simultaneous cholesterol and phospholipid superlattices has intriguing implications in lipid homeostasis of eukaryote membranes.

## Acknowledgments

This work was supported by the NIH Grant (GM078899-01) given to B.C. and the Robert A. Welch Research Foundation Grant (D-1158) and the NIH Grant (GM090897-01) given to K.H.C.

## References and Notes

1. Simons K, Ehehalt R. Cholesterol, lipid rafts, and disease. J Clin Invest. 2002; 110:597. [PubMed: 12208858]
2. Simons K, Ikonen E. Functional rafts in cell membranes. Nature. 1997; 387:569. [PubMed: 9177342]
3. Lingwood D, Simons K. Lipid rafts as a membrane-organizing principle. Science. 2010; 327:46. [PubMed: 20044567]
4. McConnell HM, Radhakrishnan A. Condensed complexes of cholesterol and phospholipids. Biochim Biophys Acta. 2003; 1610:159. [PubMed: 12648771]
5. Chong PL, Zhu W, Venegas B. On the lateral structure of model membranes containing cholesterol. Biochim Biophys Acta. 2009; 1788:2. [PubMed: 19010302]
6. Somerharju P, Virtanen JA, Cheng KH, Hermansson M. The superlattice model of lateral organization of membranes and its implications on membrane lipid homeostasis. Biochim Biophys Acta. 2009; 1788:12. [PubMed: 19007747]
7. Parker A, Miles K, Cheng KH, Huang J. Lateral distribution of cholesterol in dioleoylphosphatidylcholine lipid bilayers: cholesterol-phospholipid interactions at high cholesterol limit. Biophys J. 2004; 86:1532. [PubMed: 14990480]

8. Chong PL, Sugar IP. Fluorescence studies of lipid regular distribution in membranes. Chem Phys Lipids. 2002; 116:153. [PubMed: 12093540]
9. Cannon B, Heath G, Huang J, Somerharju P, Virtanen JA, Cheng KH. Time-resolved fluorescence and fourier transform infrared spectroscopic investigations of lateral packing defects and superlattice domains in compositionally uniform cholesterol/phosphatidylcholine bilayers. Biophys J. 2003; 84:3777. [PubMed: 12770884]
10. Virtanen JA, Cheng KH, Somerharju P. Phospholipid composition of the mammalian red cell membrane can be rationalized by a superlattice model. Proc Natl Acad Sci US A. 1998; 95:4964.
11. Cheng KH, Virtanen J, Somerharju P. Fluorescence studies of dehydroergosterol in phosphatidylethanolamine/phosphatidylcholine bilayers. Biophys J. 1999; 77:3108. [PubMed: 10585932]
12. Cheng KH, Ruonala M, Virtanen J, Somerharju P. Evidence for superlattice arrangements in fluid phosphatidylcholine/phosphatidylethanolamine bilayers. Biophys J. 1997; 73:1967. [PubMed: 9336192]
13. Cannon B, Lewis A, Metze J, Thiagarajan V, Vaughn MW, Somerharju P, Virtanen J, Huang J, Cheng KH. Cholesterol supports headgroup superlattice domain formation in fluid phospholipid/cholesterol bilayers. J Phys Chem B. 2006; 110:6339. [PubMed: 16553452]
14. Cheng KH, Cannon B, Metze J, Lewis A, Huang J, Vaughn MW, Zhu Q, Somerharju P, Virtanen J. Lipid headgroup superlattice modulates the activity of surface-acting cholesterol oxidase in ternary phospholipid/cholesterol bilayers. Biochemistry. 2006; 45:10855. [PubMed: 16953571]
15. Schuck S, Honsho M, Ekroos K, Shevchenko A, Simons K. Resistance of cell membranes to different detergents. Proc Natl Acad Sci US A. 2003; 100:5795.
16. London E, Brown DA. Insolubility of lipids in triton X-100: physical origin and relationship to sphingolipid/cholesterol membrane domains (rafts). Biochim Biophys Acta. 2000; 1508:182. [PubMed: 11090825]
17. Tokumasu F, Jin AJ, Feigenson GW, Dvorak JA. Nanoscopic lipid domain dynamics revealed by atomic force microscopy. Biophys J. 2003; 84:2609. [PubMed: 12668469]
18. Feigenson GW, Buboltz JT. Ternary phase diagram of dipalmitoyl-PC/dilauroyl-PC/cholesterol: nanoscopic domain formation driven by cholesterol. Biophys J. 2001; 80:2775. [PubMed: 11371452]
19. Chiang YW, Shimoyama Y, Feigenson GW, Freed JH. Dynamic molecular structure of DPPC-DLPC-cholesterol ternary lipid system by spin-label electron spin resonance. Biophys J. 2004; 87:2483. [PubMed: 15454445]
20. Silvius JR, del Giudice D, Lafleur M. Cholesterol at different bilayer concentrations can promote or antagonize lateral segregation of phospholipids of differing acyl chain length. Biochemistry. 1996; 35:15198. [PubMed: 8952467]
21. Kingsley PB, Feigenson GW. The synthesis of a perdeuterated phospholipids: 1,2-dimyristoyl-sn-glcero-3-phosphocholine-d72. Chem Phys Lipids. 1979; 24:135.
22. Huang J, Buboltz JT, Feigenson GW. Maximum solubility of cholesterol in phosphatidylcholine and phosphatidylethanolamine bilayers. Biochim Biophys Acta. 1999; 1417:89. [PubMed: 10076038]
23. Buboltz JT, Feigenson GW. A novel strategy for the preparation of liposomes: rapid solvent exchange. Biochim Biophys Acta. 1999; 1417:232. [PubMed: 10082799]
24. Ali MR, Cheng KH, Huang J. Assess the nature of cholesterol-lipid interactions through the chemical potential of cholesterol in phosphatidylcholine bilayers. Proc Natl Acad Sci US A. 2007; 104:5372.
25. Gratton E, Jameson DM, Hall RD. Multifrequency phase and modulation fluorometry. Annu Rev Biophys Bioeng. 1984; 13:105. [PubMed: 6378065]
26. Cheng KH. Fluorescence depolarization study of lamellar liquid crystalline to inverted cylindrical micellar phase transition of phosphatidylethanolamine. Biophys J. 1989; 55:1025. [PubMed: 2765643]
27. Cannon B, Lewis A, Metze J, Thiagarajan V, Vaughn MW, Somerharju P, Virtanen J, Huang J, Cheng KH. Cholesterol supports headgroup superlattice domain formation in fluid phospholipid/cholesterol bilayers. J Phys Chem B. 2006; 110:6339. [PubMed: 16553452]

28. Lakowicz JR, Maliwal BP. Construction and performance of a variable-frequency phase-modulation fluorometer. Biophys Chem. 1985; 21:61. [PubMed: 3971026]
29. Zannoni C, Arcioni A, Cavatarta P. Fluorescence depolarization in liquid crystals and membrane bilayers. Chem Phys Lipids. 1983; 32:179.
30. Valeur, B. Molecular Fluorescence. Wiley-VCH; New York: 2002. Estimation by means of fluorescent probes; p. 226
31. Van der Meer BW, Cheng KH, Chen SY. Effects of lateral diffusion on the fluorescence anisotropy in hexagonal lipid phases. I. Theory. Biophys J. 1990; 58:1517. [PubMed: 2275966]
32. Kodati VR, Lafleur M. Comparison between orientational and conformational orders in fluid lipid bilayers. Biophys J. 1993; 64:163. [PubMed: 8431540]
33. Ferguson, GA. Statistical analysis in psychology and education. 3. McGraw-Hill; New York: 1971. Statistical analysis in psychology and education; p. 41
34. Cannon B, Lewis A, Metze J, Thiagarajan V, Vaughn MW, Somerharju P, Virtanen J, Huang J, Cheng KH. Cholesterol Supports Headgroup Superlattice Domain Formation in Fluid Phospholipid/Cholesterol Bilayers. J Phys Chem B. 2006; 110:6339. [PubMed: 16553452]
35. Chong PLG, Olsher M. Fluorescence studies of the existence and functional importance of regular distribution in liposomal membranes. Soft Mater. 2004; 2:85.
36. Venegas B, Sugar IP, Chong PL. Critical factors for detection of biphasic changes in membrane properties at specific sterol mole fractions for maximal superlattice formation. J Phys Chem B. 2007; 111:5180. [PubMed: 17441759]
37. Qiu L, Lewis A, Como J, Vaughn MW, Huang J, Somerharju P, Virtanen J, Cheng KH. Cholesterol modulates the interaction of beta-amyloid peptide with lipid bilayers. Biophys J. 2009; 96:4299. [PubMed: 19450500]
38. Kaiser RD, London E. Location of diphenylhexatriene (DPH) and its derivatives within membranes: comparison of different fluorescence quenching analyses of membrane depth. Biochemistry. 1998; 37:8180. [PubMed: 9609714]
39. Zhu Q, Cheng KH, Vaughn MW. Molecular dynamics studies of the molecular structure and interactions of cholesterol superlattices and random domains in an unsaturated phosphatidylcholine bilayer membrane. J Phys Chem B. 2007; 111:11021. [PubMed: 17718554]
40. Silvius JR, Leventis R. Spontaneous interbilayer transfer of phospholipids: dependence on acyl chain composition. Biochemistry. 1993; 32:13318. [PubMed: 8241188]
41. Haimi P, Hermansson M, Batchu KC, Virtanen JA, Somerharju P. Substrate efflux propensity plays a key role in the specificity of secretory A-type phospholipases. J Biol Chem. 2010; 285:751. [PubMed: 19887372]
42. Sugahara M, Uragami M, Regen SL. Selective sterol-phospholipid associations in fluid bilayers. J Am Chem Soc. 2002; 124:4253. [PubMed: 11960454]
43. Pasenkiewicz-Gierula M, Rog T, Kitamura K, Kusumi A. Cholesterol effects on the phosphatidylcholine bilayer polar region: a molecular simulation study. Biophys J. 2000; 78:1376. [PubMed: 10692323]
44. Pandit SA, Bostick D, Berkowitz ML. Complexation of phosphatidylcholine lipids with cholesterol. Biophys J. 2004; 86:1345. [PubMed: 14990465]
45. Op Den Kamp JAF, Kauerz MT, Van Deenen LLM. Action of pancreatic phospholipase A2 on phosphatidylcholine bilayers in different physical states. Biochim Biophys Acta. 1975; 406:169. [PubMed: 1191645]
46. Lange Y, Steck TL. Cholesterol homeostasis and the escape tendency (activity) of plasma membrane cholesterol. Prog Lipid Res. 2008; 47:319. [PubMed: 18423408]

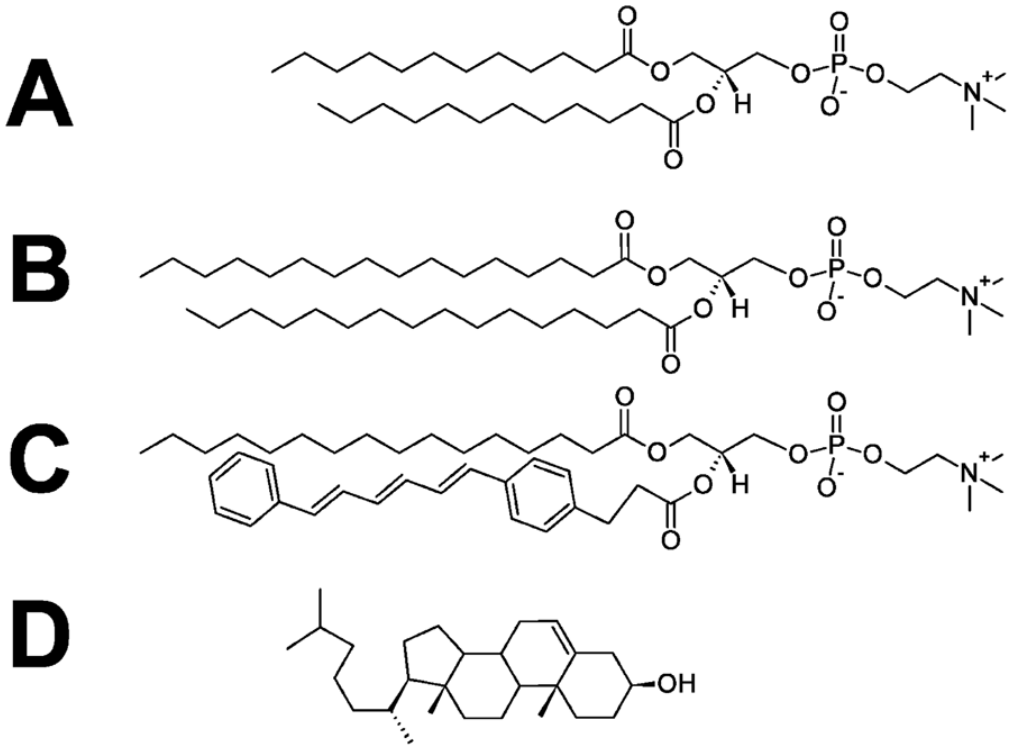


**Figure 1.**
Molecular structures of DLPC (A), DPPC (B), DPH-PC (C), and cholesterol (D).

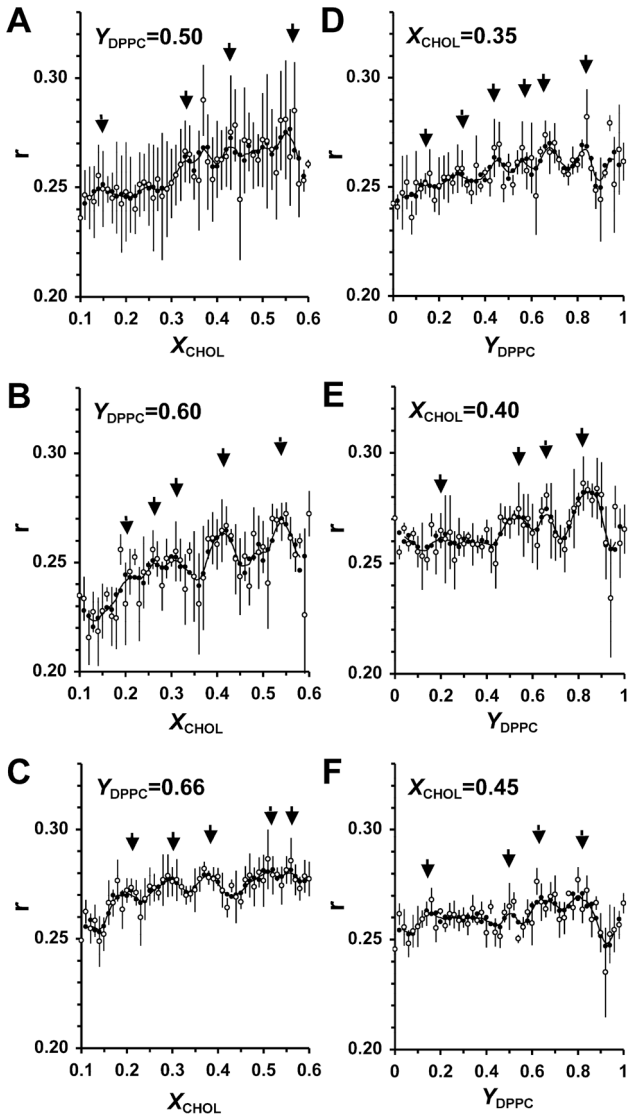


**Figure 2.**

Steady-state anisotropy *r* of DPH-PC in DPPC/DLPC/CHOL bilayers versus CHOL/lipid mole ratio ($X_{CHOL}$) (left column) plots at 23 °C for a fixed DPPC/PC mole ratio ($Y_{DPPC}$) of 0.50 (A), 0.60 (B), and 0.66 (C). The *r* versus $Y_{DPPC}$ (right column) plots at 23 °C for a fixed $X_{CHOL}$ of 0.35 (D), 0.40 (E), and 0.45 (F) are also shown. Raw averaged data from parallel samples (○), one-pass three-point moving averages (●) and two-pass three-point moving averages (line) are presented. The arrows indicated the identified peaks (see Materials and Methods). Bars indicate standard errors. The data represent averages of measurements from three ($N$ = 3) parallel and independently prepared liposome preprations for all samples except the plot with a fixed $X_{CHOL}$ of 0.40 in which $N$ = 4.

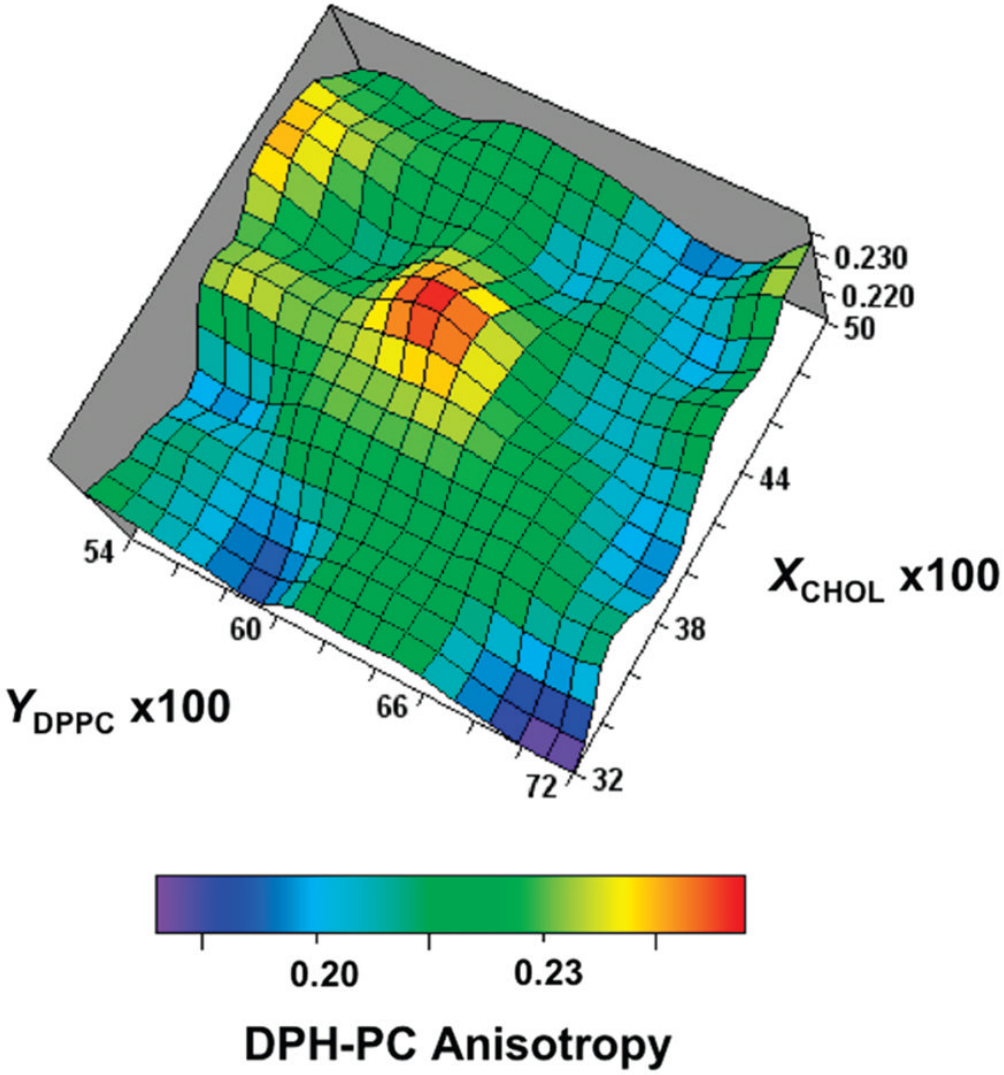


**Figure 3.**
Three-dimensional surface plot of steady-state anisotropy of DPH-PC in DPPC/DLPC/CHOL bilayers versus $X_{CHOL}$ and $Y_{DPPC}$. The data represent averages of measurements from three parallel and independently prepared liposome preparations.

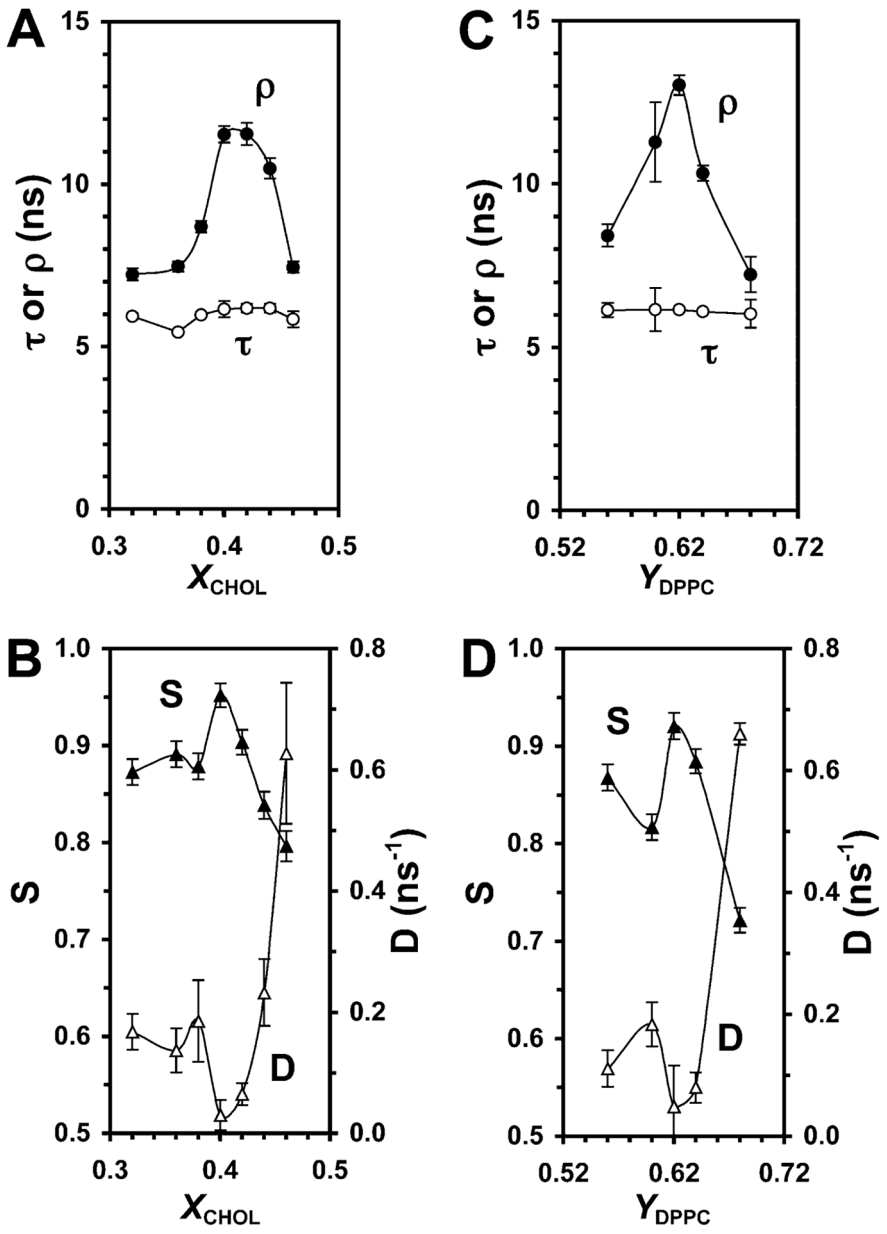


**Figure 4.**

Fluorescence intensity decay lifetime ($\tau$) and rotational correlation time $\rho$ (A or B) and orientational order $S$ and rotational diffusion coefficient $D$ (C or D) of DPH-PC in DPPC/DLPC/CHOL at 23 °C versus versus $X_{CHOL}$ or $Y_{DPPC}$. The data represent averages of measurements from three parallel and independently prepared liposome preprations. See legends of Figure 2 for other details.

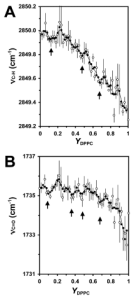


**Figure 5.**

Peak of the FTIR vibrational frequency band of C–H (A) and C=O (B) of phospholipids in DPPC/DLPC/CHOL bilayers at 23 °C versus $Y_{DPPC}$ for $X_{CHOL}$ = 0.40. The data represent averages of measurements from five parallel and independently prepared liposome preprations. See legends of Figure 2 for other details.

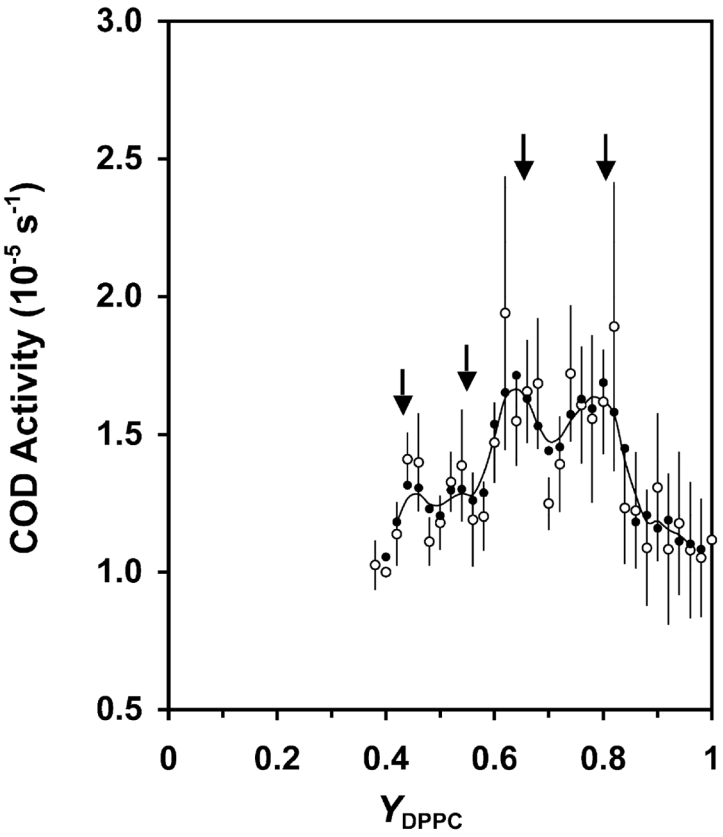


**Figure 6.**
COD activity at 23 °C versus $Y_{DPPC}$ in DPPC/DLPC/CHOL liposomes for for $X_{CHOL}$ = 0.40. The data represent averages of measurements from 11 parallel and independently prepared liposome preprations. See legends of Figure 2 for other details.

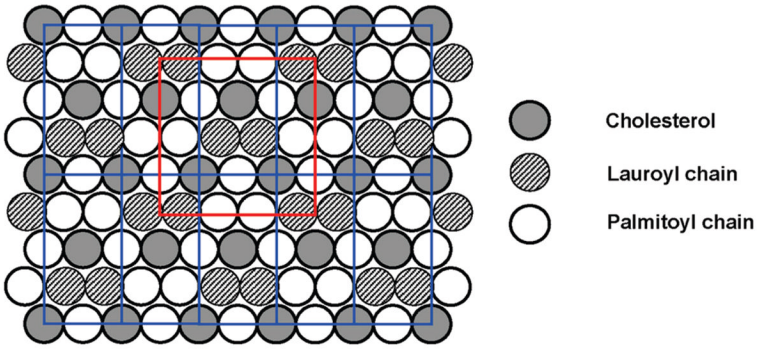


**Figure 7.**

Proposed organizations of simultaneous cholesterol and acyl chain superlattices in DPPC/DLPC/CHOL bilayers at the theoretical critical compositions of $X_{CHOL}$ = 0.40 and $Y_{DPPC}$= 0.67. Ten unit cells (blue squares) of Cholesterol SL (CHOL/PC-SL) in centered rectangular symmetry and one unit cell (red square) of Phospholipid SL (DPPC/DLPC-SL) also in centered rectangular symmetry with the double-chains of DLPC as the host are shown.

## TABLE 1

Comparison of Critical Mole Fration $X_{CHOL}$ from Steady-State Fluorescence Anisotropy Measurements of DPH-PC with $X^{HX}$, $X^{CR}$, or $X^{R}$ Values Predicted by the Cholesterol Superlatitice Model in Ternary Mixtures of DPPC/DLPC/CHOL at a Fixed DPPC/PC Ratio of $Y_{DPPC}$ = 0.50, 0.60, and 0.66[a]

| $X^{HX}$, $X^{CR}$, or $X^{R}$ | $Y_{DPPC}$ = 0.50 | $Y_{DPPC}$ = 0.60 | $Y_{DPPC}$ = 0.66 |
|---|---|---|---|
| $0.15^{HX,CR,R}$ | 0.15 (70, 70) | | |
| $0.20^{HX,CR}$ | | 0.20 (93, 84) | 0.20 (95, 78) |
| $0.22^{CR,R}$ | | | |
| $0.25^{HX,CR}$ | | 0.26 (86, 84) | |
| $0.33^{CR}$ | 0.33 (73, 73) | 0.31 (79, 77) | 0.30 (85, 76) |
| $0.40^{HX,CR,R}$ | 0.43 (75, 82) | 0.42 (87, 96) | 0.38 (96, 98) |
| $0.50^{HX,CR}$ | | | 0.52 (75, 76) |
| | 0.56[b] (76, 82) | 0.54[b] (87, 94) | 0.56[b] (76, 75) |

[a] The critical mole fractions are identified from the peaks of the two-pass three-point running averages of the raw data (see Figure 2 and Materials and Methods). The probability of significance ($P_R$, $P_L$) of each critical molar fraction based on the *t*-test (see Materials and Methods) is also shown besides each critical mole fracton.

[b] Critical mole fractions that do not agree (±0.03) with $X^{HX}$, $X^{CR}$, or $X^{R}$ values.

## TABLE 2

Comparison of Critical Mole Fration $Y_{DPPC}$ from Steady-State Fluorescence Anisotropy Measurements of DPH-PC with $Y^{HX}$, $Y^{CR}$, or $Y^{R}$ Values Predicted by the Headgroup Superlatitice Model for Ternary Mixtures of DPPC/DLPC/CHOL at a Fixed CHOL/Lipid Ratio of $X_{CHOL}$ = 0.35, 0.40, and 0.45[a]

| $Y^{HX}$, $Y^{CR}$, or $Y^{R}$ | $X_{CHOL}$ = 0.35 | $X_{CHOL}$ = 0.40 | $X_{CHOL}$ = 0.45 |
|---|---|---|---|
| $0.14^{HX,CR}$, $0.17^{R}$ $0.20^{CR}$ | 0.14 (91, 83) | 0.20 (89, 79) | 0.16 (83, 93) |
| $0.25^{HX,CR,R}$ | | | |
| $0.33^{HX,CR}$ | 0.30 (84, 78) | | |
| | 0.46[b] (87, 90) | | |
| $0.50^{R}$ | | 0.52 (91, 83) | 0.50 (94, 93) |
| | 0.56[b] (86, 82) | | |
| $0.67^{HX,CR}$ | 0.68 (88, 88) | 0.66 (94, 97) | 0.64 (97, 91) |
| $0.75^{HX,CR,R}$ | | | |
| $0.80^{CR}$, $0.83^{R}$, $0.86^{HX,CR}$ | 0.84 (89, 91) | 0.84 (95, 88) | 0.82 (91, 92) |

[a] See the footnote of Table 1 for details.

[b] Critical mole fractions that do not agree (±0.03) with $Y^{HX}$, $Y^{CR}$, or $Y^{R}$ values.

## TABLE 3

Comparison of Critical Mole Fration $Y_{DPPC}$ from FTIR[a] and COD Activity[b] Measurements with $Y^{HX}$, $Y^{CR}$, or $Y^{R}$ Values Predicted by the Headgroup Superlatitice Model for Ternary Mixtures of DPPC/DLPC/CHOL at a Fixed CHOL/Lipid ratio of $X_{CHOL}$ = 0.40

| $Y^{HX}$, $Y^{CR}$, or $Y^{R}$ | $\nu_{C-H}$ | $\nu_{C=O}$ | COD |
|---|---|---|---|
| $0.11–0.13^{HX,CR,R}$ | 0.12 (77, 82) | 0.10 (99, 99) | |
| $0.14^{HX,CR}$, $0.17^{R}$, $0.20^{CR}$ | | | |
| $0.25^{HX,CR,R}$ | | | |
| $0.33^{HX,CR}$ | | 0.36 (89, 90) | |
| | | | $0.44^{b}$ (99, 90) |
| $0.50^{R}$ | 0.48 (84, 96) | 0.48 (85, 93) | |
| | | | $0.54^{b}$ (85, 80) |
| $0.67^{HX,CR}$ | 0.68 (75, 86) | 0.68 (95, 99) | 0.64 (94, 90) |
| $0.75^{HX,CR,R}$ | | | |
| $0.80^{CR}$, $0.83^{R}$, $0.86^{HX,CR}$ | | | 0.80 (90, 88) |
| $0.87–0.89^{HX,CR,R}$ | | | |

[a] The critical mole fractions are identified from the dips or peaks of the two-pass three-point running averages of the raw data of FTIR or COD measurements, respecitively (see Figure 5 and Materials and Methods). The parentheses besides each critical mole fraction denotes the probability of significance (see footnote of Table 1).

[b] See the footnote of Table 2 for details.